Performance Analysis of Frequency and Voltage Control from PV/BESS Unit in Islanded Microgrid Towards Load Changes

Luana C. S. Soares [*] **Pedro A. de Alcântara** [*]
Lindemberg R. de Lima [**] **Camila M. V. Barros** [***]
Luciano S. Barros [***]

[*] *Electrical Engineering Graduate Program, Federal University of Paraiba, PB (e-mails: luana.soares@cear.ufpb.br, pedro.alcantra@cear.ufpb.br).*
[**] *Mathematics and Computational Modeling Graduate Program, Federal University of Paraiba, PB (e-mail: lindemberg.roberto@academico.ufpb.br)*
[***] *Computer System Department, Federal University of Paraiba, PB (e-mails: camila.barros@ci.ufpb.br, lsalesbarros@ci.ufpb.br)*

Abstract: Microgrids based on photovoltaic array supplying do not have capacity to compensate imbalances between generation and load demand, which can occur in islanded operation and cause voltage and frequency deviations. Therefore, battery energy storage systems are inserted to help in microgrid regulation. Grid-forming droop control is applied for PV/battery hybrid units to be capable of controlling voltage and frequency in the islanded mode of the microgrid. The objective of this article is to present a performance analysis of this control, considering several load levels in microgrid including the ones when battery energy storage systems state of charge limits are reached, what is followed by its turning off. For this purpose, simulations were conducted in the MATLAB/Simulink environment using a simplified low voltage system. The results point out to the effectiveness of the control when the battery is connected to the system despite load changes, regulating voltage and frequency levels. However, with the battery disconnection, the control is no longer able to regulate microgrid operation.

Keywords: Three-phase microgrid; islanded operation; hybrid photovoltaic/battery unit; grid-forming droop control; state of charge-based control.

1. INTRODUCTION

Microgrids can be comprehended as power systems on a smaller scale that aim to facilitate the integration of distributed generation into the electrical system (Lasseter, 2002), such as photovoltaic (PV) generation. In addition to distributed generation, microgrids also have batteries and loads in their composition. These grids can operate connected to the main grid or in islanded mode and can be single/three-phase, in direct or alternating current, or even a combination of both, when they are called hybrid microgrids (Unamuno and Barrena, 2015). In Fig. 1 it is possible to observe the microgrid configuration studied in this paper and its elements, described in Section 2. The connection of the microgrid to the main grid is made by the circuit breaker (CB), which represents the connection switch to the grid. When the microgrid is connected, the CB is closed and the microgrid works in connected mode to inject or absorb power from the grid. When in islanding mode, the CB is open and the microgrid operates independently, being responsible for balancing its power generation with its connected loads (Olivares et al., 2014). Since PV supply does not have the capacity to compensate imbalances between generation and load demand, battery energy storage systems (BESS) are connected to the MG to help regulate the frequency and voltage as they are efficient systems with quick response to disturbances. BESS can be connected to the microgrid as individual units or can be connected together to the PV unit, forming a hybrid generation unit (Fakham et al., 2011), being a more cost effective configuration.

In islanded mode, the proper functioning of the control system for power management in the microgrid is essential. Control strategies can be centralized or decentralized. The centralized control strategy relies on communication between units and microgrid loads, which reduces system reliability. On the other hand, the decentralized control method requires only local measurements, such as droop control, and can also use non-critical communications to achieve other goals such as restoring voltage and frequency variations (Karimi et al., 2017b; Guerrero et al., 2011). The droop control is one of the most discussed and applied strategies to the operation of microgrids. According to Netto Moura (2019), this method is effective for power sharing and is attractive as it does not depend on communication between the inverters of the different units. This work adopts a grid-forming (GFM) droop control strategy

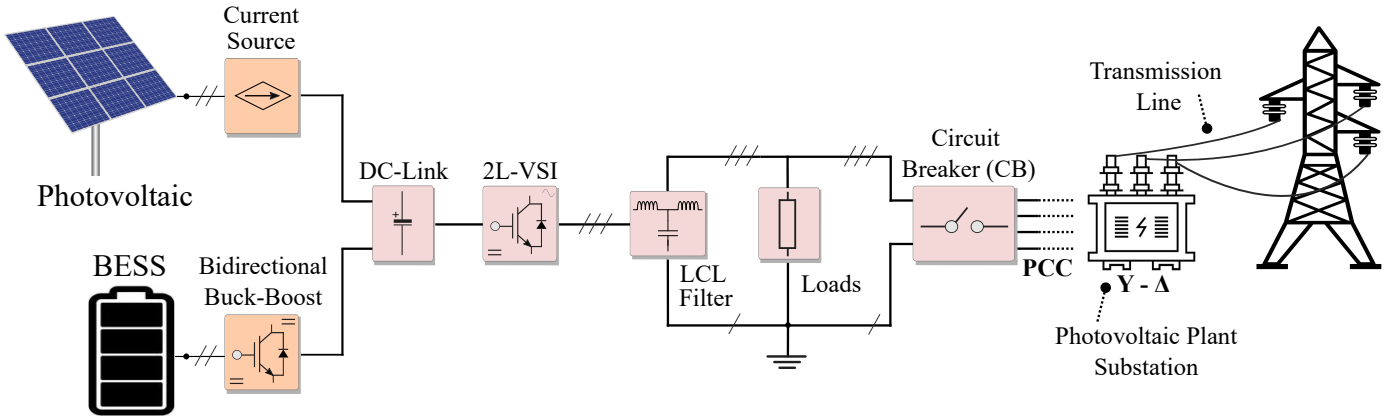

Figure 1. Three-phase microgrid architecture with hybrid source unit.

that has been extensively used in microgrid configurations to actively control the frequency and voltage output (Pattabiraman et al., 2018). The strategy, based on Karimi et al. (2017b), makes it possible to have a proper power management in the microgrid in the face of load changes in MG.

This article analyzes the behavior of a three-phase microgrid when BESS is applied to mitigate voltage and frequency deviations in moments of unbalance between generation and load, in addition to controlling the terminal voltage of this system at a safe value. The main goal is to present a performance analysis of the grid-forming control seen in Karimi et al. (2017b) but exposing the voltages behavior among the variations in the system. In addition, the microgrid will also be analyzed when BESS reaches its SoC limit and needs to be disconnected from the system. In this microgrid, composed of a hybrid unit with PV generation and battery, the decentralized method strategy controls the power delivered to the loads.

The paper is organized as follows: in Section 2, the structure of the three-phase microgrid with a hybrid generation unit is presented. In Section 3 the control systems used for connected and islanded modes are presented. Section 4 presents the results of the simulations performed. Section 5 ends the article with the conclusion.

2. MICROGRID ARCHITECTURE AND MODELING

The three-phase microgrid analyzed in this work is illustrated in Fig. 1 and all its power and voltage characteristics are described in Table 1. In this configuration, it is connected to the grid through a Δ-Y transformer and a CB. The three-phase unit (TPU) is composed of PV and BESS generation, and loads are connected to the TPU interface inverter terminal busbar. The inverter is connected to the common coupling point (PCC) through an LCL filter, which helps ensure that the output impedance of unit is mainly inductive. The BESS is connected to the dc-link through a bidirectional buck-boost converter and the PV array is connected through a boost converter.

The two-level voltage source inverter (VSI) topology adopted for the TPU, chosen for its simplicity and wide use, is seen in Barbi (2007). The bidirectional buck-boost converter was based in Kazimierczuk (2015) and an ideal current source represents the PV. Using an ideal current source ensures that a constant power is injected into the microgrid even in islanding situations, which is the role that the maximum power point tracker (MPPT) plays when working with PV. The lithium-ion battery model presented in Silva et al. (2021) was adopted to represent the BESS. It is based on the open circuit terminal voltage versus SoC relation, experimentally estimated by Baronti et al. (2013, 2014).

3. ISLANDED MODE CONTROL

The microgrid seen in this work has the ability to operate in connected and islanded modes due to the implemented control systems. In this work, the behavior of the microgrid when operating in islanded mode will be analyzed, where initially the microgrid is connected to the grid and then the CB will switch to the islanded mode.

In connected mode, the VSI control is responsible for keeping the dc-link voltage as close as possible from its setpoint in face of variations in the system. This control system can be seen in Barros and Barros (2017).

The grid-forming droop control structure used to operate in islanded mode is based on Karimi et al. (2017b,a) and is illustrated in Fig. 2, where i_{fa}, i_{fb} and i_{fc} are the currents that flow through each phase before the LCL filter; L_f, C_f and L_0 are the LCL filter components; i_a, i_b and i_c are the currents in PCC; V_{abc} are the voltages across the capacitor of the LCL filter, and $P_{out-abc}$ and $Q_{out-abc}$ are the active and reactive power in PCC, respectively. This control comprises: power calculation (Akagi et al., 1984), reference voltage amplitude and frequency calculation, AC voltage control loop and PWM.

The reference voltage frequency is given by the $P - f$ droop function and the amplitude is given by $Q - v$ droop function. The proportional-resonant (PR) control for AC voltage control was based on Vasquez et al. (2013). The dc-link voltage control was implemented based on the bidirectional buck-boost converter control seen in Mahmood et al. (2015); Matos et al. (2015).

In this scenario, the microgrid will operate in the following modes:

- **Mode 1**: Grid connected operation, when the grid absorbs excess power or injects it into the microgrid

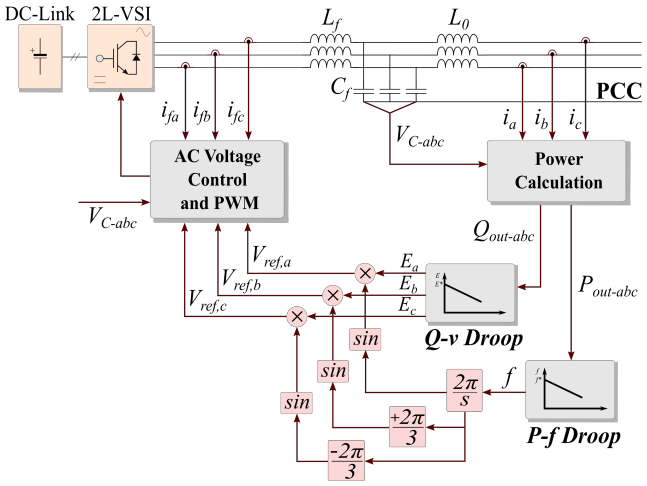

Figure 2. VSI control structure for islanded mode. Adapted from Karimi et al. (2017b,a).

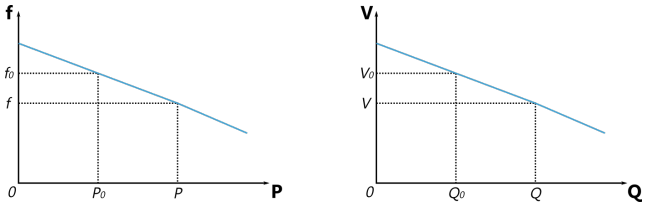

Figure 3. Traditional droop control curves. Adapted from Zhang et al. (2018).

and the VSI control is able to regulate the dc-link voltage;

- **Mode 2**: In islanded operation, when total MG load is larger than PV power and battery provides the necessary surplus load power. In this case, bidirectional buck-boost converter regulates the dc-link voltage and VSI is droop-controlled;
- **Mode 3**: In islanded operation, when total MG load is less than PV power and battery absorbs the surplus PV power. In this case, bidirectional buck-boost converter regulates the dc-link voltage and VSI is droop-controlled;
- **Mode 4**: In islanded operation, when battery reaches its SoC limit and needs to be disconnected from the system. The bidirectional buck-boost converter is unable to control the dc-link voltage.

3.1 Droop control

The microgrid adopts the droop control strategy to allow its output to be automatically adjusted according to the given power characteristic (Zhang et al., 2018). With this mechanism, the PV will be able to respond to system dynamics, such as load changes. Traditional droop control curves are illustrated in Fig. 3, and its equations are:

$$f = f_0 + m \cdot (P_0 - P), \quad (1)$$
$$V = V_0 + n \cdot (Q_0 - Q), \quad (2)$$

where f is the MG frequency, f_0 is the nominal frequency, m is the $P-f$ droop coefficient, P is the measured active power, P_0 is the nominal power, V is the terminal busbar voltage amplitude, V_0 is the nominal voltage, n is the $Q-v$ droop coefficient, Q is the measured reactive power and Q_0 is the nominal reactive power.

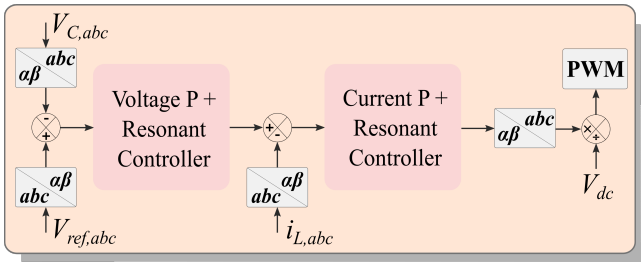

Figure 4. VSI inner control loop. Adapted from Vasquez et al. (2013).

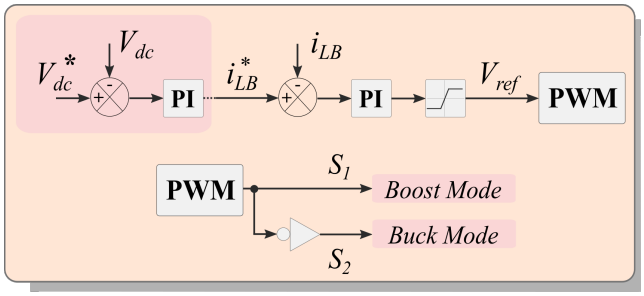

Figure 5. Controller block diagram of the dc-dc converter.

3.2 Proportional-resonant controller

The closed loop PR controller allows a sinusoidal reference signal with frequency ω_0 to be reapplied to the system output, guaranteeing zero error at this frequency in steady state. In Vasquez et al. (2013) is seen the structure of the resonant control for the three-phase VSI, developed in the synchronous reference frame with $abc/\alpha\beta$ transformation. The voltages generated by the droop control go to the PR control, where the control of sinusoidal voltages and currents is performed. Fig. 4 illustrates the configuration of the resonant control, where $V_{C,abc}$ are the voltages across the capacitor of the LCL filter, $V_{ref,abc}$ are the voltages genereted by the droop control, $i_{L,abc}$ are the currents that flow through each phase and V_{dc} is the dc-link voltage measurement.

The VSI control strategy with a PR controller including the adjustment of the control parameters can be seen in detail in Vasquez et al. (2013).

3.3 Control of the bidirectional buck-boost converter

The bidirectional buck-boost converter allows the charge and discharge of the battery and is also used to control the dc-link voltage. In Matos et al. (2015) and Mahmood et al. (2015) the dynamic equations of control and controller design are seen and Fig. 5 illustrates its block diagram. The control parameters adjustments can also be seen in Mahmood et al. (2015). The dc-link voltage control is initially performed generating a i_{LB} current reference, which is the current that flows through the inductor of the bidirectional buck-boost converter. The output of this control is the PWM voltage reference responsible for controlling the switch states of the bidirectional buck-boost converter, represented by S_1 and S_2.

In islanded mode, since the PV works in maximum power and there is no power assistance from the grid, the battery unit is responsible for voltage regulation injecting or absorbing active power into the microgrid. This action makes it possible to regulate the dc-link voltage.

4. SIMULATION RESULTS

The microgrid system was built according to the parameters presented in Table 1 and the simulations were carried out in the MATLAB Simulink environment. The control parameters for both modes are in Tables A.1 and A.2 in the Appendix A. A constant impedance model was used to define the loads. Their resistances are summarized in Tables 2 and 3.

Table 1. Simulation Parameters.

Parameter	Symbol	Value	Unit
Nominal Voltage	E*	127	V_{rms}
Nominal Frequency	f_0	60	Hz
Nominal DC-Link Voltage	V_{dc}	300	V
PV Power	P_{pv}	1000	W
Converter-Side Inductance	L_f	0.5	mH
Filter Capacitance	C_f	9	μF
Grid-Side Inductance	L_0	0.5	mH
Battery Energy Capacity	E_{bat}	20	Ah
Battery Voltage	V_{bat}	155	V

The battery cell data was obtaned in Baronti et al. (2013) and the proper voltage was achieved by placing these cells in series. To demonstrate the control performance and the battery role in the regulation of frequency and voltage of the microgrid, tests were carried out in three different load scenarios with a 4% unbalance between each phase, starting the simulation in connected mode and islanding it in t = 1 s.

In an islanded microgrid, the frequency and voltage directly depend on the balance between generation and load. Therefore, they may vary if this criterion is not fully met. This simulation does not use the secondary microgrid control seen in Guerrero et al. (2013) to compensate for frequency and amplitude deviations. If there is a big imbalance in the microgrid, the frequency and voltage can go out of their limits due to the absence of this control interference.

Three scenarios have been tested, in the first one the PV power is larger than the load plus system losses, therefore, the battery charges to absorb the generation surplus. In this situation, the battery reaches its maximum SoC limit and is disconnected from the system. In the second scenario the PV power is less than the load plus losses in the system, therefore, the battery discharges to inject the excess power needed in the microgrid. In this situation, the battery reaches its minimum SoC limit and is disconnected from the system. The SoC limits are considered 20% and 90% based on lithium-ion battery characteristics. In the third one, a scenario is seen where there are load variations in islanded mode that force the battery to charge and discharge to supply the needs of the system and to regulate the dc-link voltage. In all the scenarios mentioned, before the disconnection of the battery, bidirectional buck-boost converter is able to regulate the dc-link voltage.

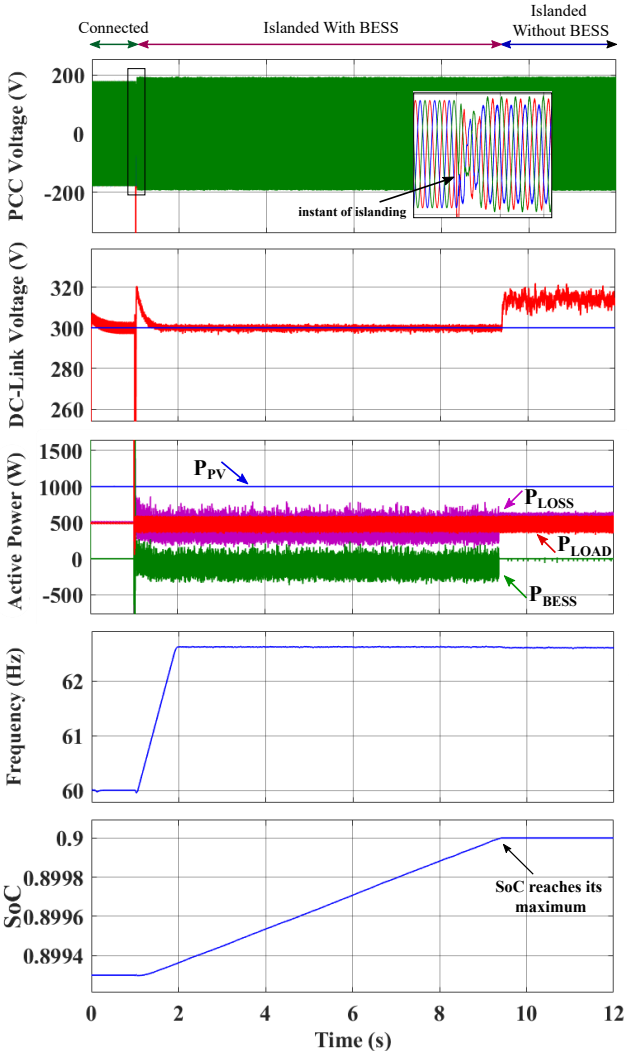

Figure 6. Scenario for a $Z_{a,b,c} = 102,\ 98.33,\ 94.3\ \Omega$ load.

4.1 First Scenario - Load Plus Losses Less Than Generation

In this scenario, a load smaller than the generation is connected until the maximum SoC limit is reached. When the battery is disconnected, there is no longer the possibility of storing the excess generation and therefore, the dc-link voltage rises so that the system balance is reached. Fig. 6 shows the graphics of the PCC voltage, dc-link voltage, active power, microgrid frequency and SoC when the impedance load is set to $Z_{a,b,c} = 102,\ 98.33,\ 94.3\ \Omega$. With battery disconnection, the PR control is able to maintain the PCC voltage, but the dc-link voltage rises.

For a $Z_{a,b,c} = 472,\ 480,\ 505\ \Omega$ load, the battery tends to absorb more power and charges faster. The dc-link also absorbs more power and presents a higher voltage after battery disconnection, causing a larger frequency variation. This behavior can be seen in Fig. 7.

This scenario was analyzed for different load values and they are summarized in Table 2. The values seen for the dc-link voltage are those obtained after the battery exit from the system. In all situations it is possible to observe that the control regulates the dc-link voltage, except when

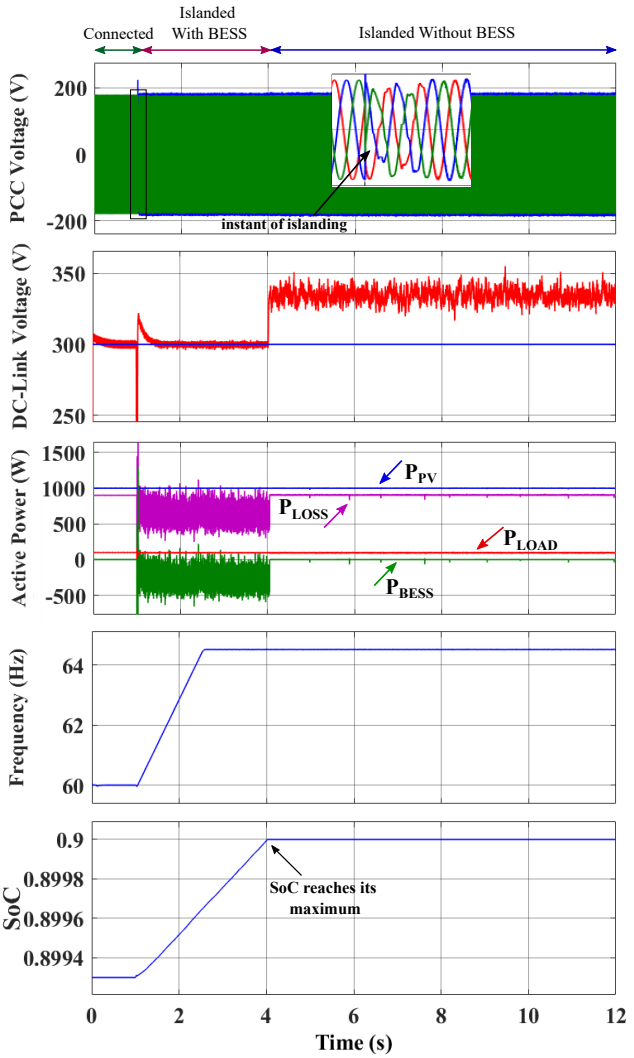

Figure 7. Scenario for a $Z_{a,b,c} = 472,\ 480,\ 505\ \Omega$ load.

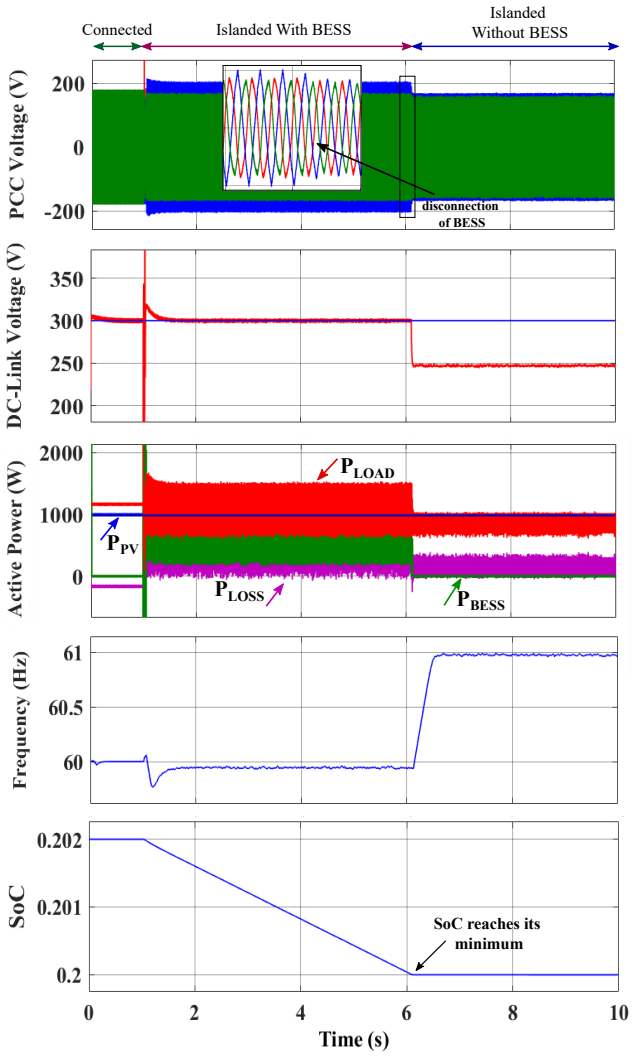

Figure 8. Scenario for a $Z_{a,b,c} = 40,\ 41.5,\ 43.25\ \Omega$ load.

the battery is disconnected from the system. PR control allows load voltages to be maintained.

Table 2. Charging Scenario.

Z_{LOAD} (a, b, c) [Ω]	P_{BESS} [W]	V_{dc} [V]	f_{max} [Hz]
102, 98.33, 94.3	-94.2	313.7	62.60
144, 148.66, 155.4	-182.6	326.6	63.43
187, 193, 201.5	-224.2	331.8	63.78
237, 248.66, 255	-232.1	333.1	64.05
472, 480, 505	-254.0	334.3	64.51

4.2 Second Scenario - Load Plus Losses Larger Than Generation

In this scenario, a load larger than the generation is connected until the minimum SoC limit is reached. Fig. 8 shows the graphics when the impedance load is set to $Z_{a,b,c} = 40,\ 41.5,\ 43.25\ \Omega$. Battery disconnection causes a decrease in the AC voltage, causing a decrease in the load power, which becomes lower than the generation power. This happens due to the fact that the load model is of constant impedance type. In response, the frequency tends to increase. This can happen in a real system for a real load, where the AC voltage decrease and consequent load decrease could be different, which would change the frequency variation.

For a $Z_{a,b,c} = 31.8,\ 33,\ 34.4\ \Omega$ impedance load, the battery injects more power in the load and then will discharge faster. The dc-link also injects more power and presents a lower voltage after battery disconnection. This behavior can be seen in Fig. 9.

This scenario was analyzed for different load values and they are summarized in Table 3. The values seen for the dc-link voltages are those obtained after the battery exit from the system and f_{min} is the nadir frequency seen at the time of islanding. In all situations it is possible to observe that the bidirectional buck-boost converter control regulates the dc-link voltage, except when the battery is disconnected from the system.

Table 3. Discharging Scenario.

Z_{LOAD} (a, b, c) [Ω]	P_{BESS} [W]	V_{dc} [V]	f_{min} [Hz]
40, 41.5, 43.25	438.4	247.1	59.78
39.2, 40, 42	473.2	244.2	59.68
39, 37.5, 36	546.5	237.1	59.42
33.6, 35, 36.4	633.2	230.3	59.10
31.8, 33, 34.4	706.6	224.6	58.82

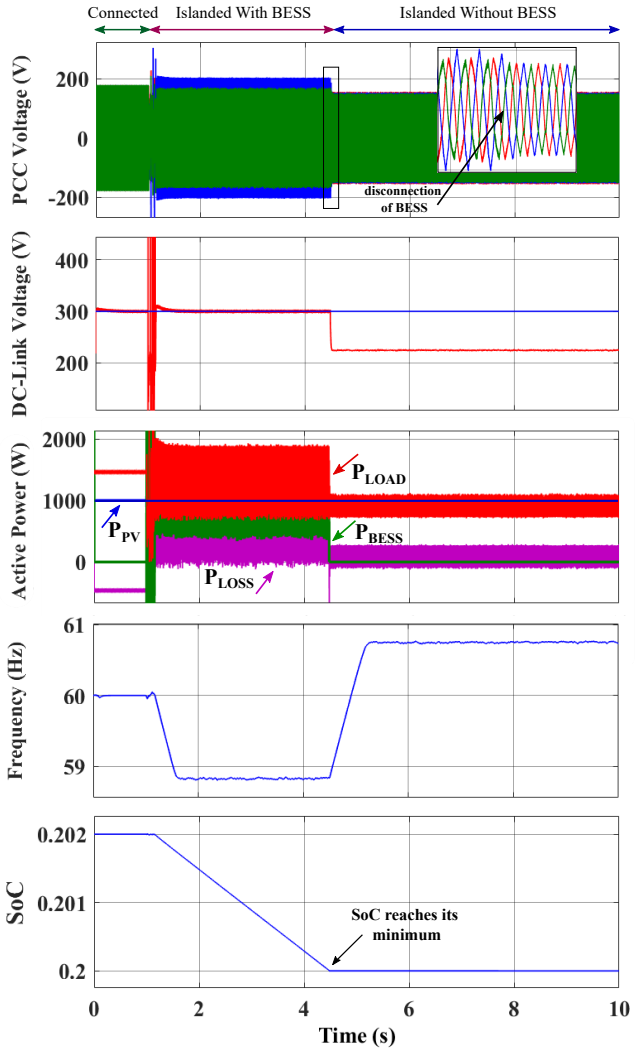

Figure 9. Scenario for a $Z_{a,b,c} = 31.8,\ 33,\ 34.4\ \Omega$ load.

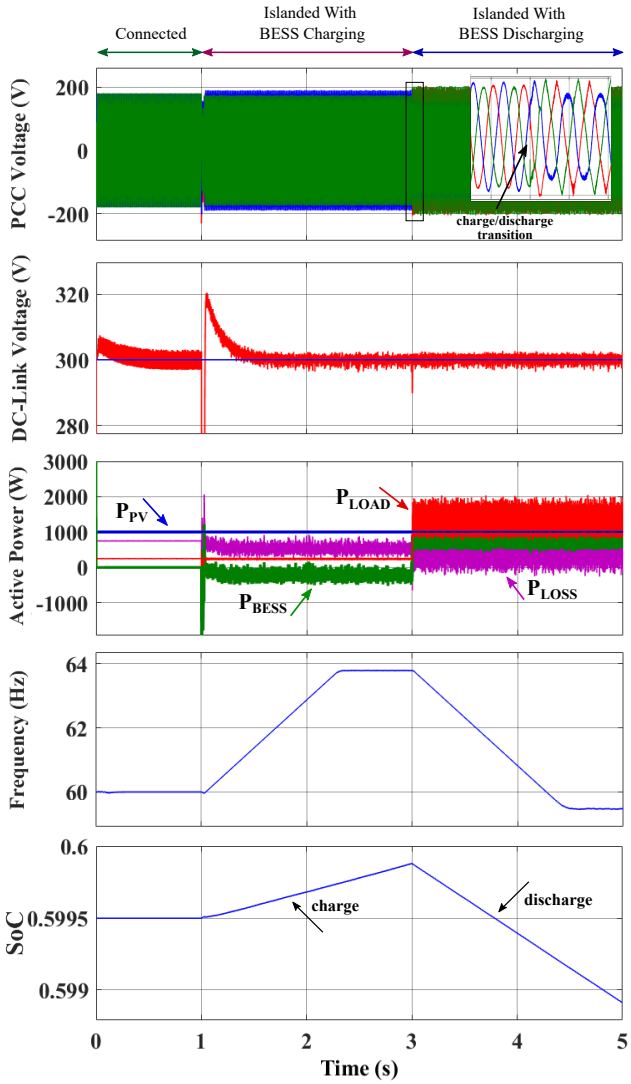

Figure 10. Scenario for a $Z_{a,b,c} = 187,\ 193,\ 201.5\ \Omega$ and $Z_{a,b,c} = 39,\ 37.5,\ 36\ \Omega$ loads.

4.3 Third Scenario

In this scenario, the behavior of the microgrid is analyzed when load is smaller or larger than the generation. In this case, the dc-link voltage is controlled despite the islanding at 1 s with load smaller and the load change at 3 s. Fig. 10 shows frequency behavior, among others.

5. CONCLUSION

This article analyzed the voltage and frequency regulation in a three-phase islanded microgrid with a hybrid photovoltaic/battery generation unit using a grid-forming droop control. This control actively generates frequency and voltage references and controls the AC voltage through an internal proportional-resonant. This enabled the microgrid to work efficiently in different situations of load variations with the battery state of charge within acceptable limits. Simulation results showed that the lithium-ion battery is able to provide voltage and frequency support when connected to the microgrid. Battery disconnection is performed within defined limits in order to increase its useful life, allowing it to work for more cycles and thus reducing system costs. However, with the disconnection, the control is no longer able to regulate dc-link voltage and consequently the AC voltage and frequency levels.

Appendix A. CONTROL PARAMETERS

The control parameters used in simulations are summarized in Tables A.1 and A.2.

Table A.1. Connected Control Parameters.

Parameter	Symbol	Value
DC-Link Voltage (PI)	K_p, K_i	250, 500
Direct Axis Current (PI)	K_p, K_i	0.15, 0.5
Quadrature Axis Current (PI)	K_p, K_i	0.5, 0.15

Table A.2. Islanded Control Parameters.

Parameter	Symbol	Value
Voltage Loop (PR)	K_{pV}, K_{iV}	500, 500
Current Loop (PR)	K_{pL}, K_{iL}	100, 100
DC-Link Voltage (PI)	K_p, K_i	0.63, 150
Bidirectional Indutor Current (PI)	K_p, K_i	0.2325, 1.57
Frequency Droop Coefficient	m	0.005
Voltage Droop Coefficient	n	1

ACKNOWLEDGEMENTS

This work was supported by the National Council for Scientific and Technological Development (CNPq) and by the Coordination for the Improvement of Higher Education Personnel (CAPES), Brazil. The authors also want to demonstrate their thankfulness to Electrical Engineering Graduate Program, to Informatic Center of UFPB and mainly to Digital System Laboratory (LASID) by the opportunity to develop this work.

REFERENCES

Akagi, H., Kanazawa, Y., and Nabae, A. (1984). Instantaneous reactive power compensators comprising switching devices without energy storage components. *IEEE Transactions on Industry Applications*, IA-20(3), 625–630. doi:10.1109/TIA.1984.4504460.

Barbi, I. (2007). *Inverter Project*. Federal University of Santa Catarina, 1 edition.

Baronti, F., Femia, N., Saletti, R., and Zamboni, W. (2014). Comparing open-circuit voltage hysteresis models for lithium-iron-phosphate batteries. In *IECON 2014 - 40th Annual Conference of the IEEE Industrial Electronics Society*, 5635–5640. doi:10.1109/IECON.2014.7049363.

Baronti, F., Zamboni, W., Femia, N., Roncella, R., and Saletti, R. (2013). Experimental analysis of open-circuit voltage hysteresis in lithium-iron-phosphate batteries. In *IECON 2013 - 39th Annual Conference of the IEEE Industrial Electronics Society*, 6728–6733. doi:10.1109/IECON.2013.6700246.

Barros, L.S. and Barros, C.M.V. (2017). An internal model control for enhanced grid-connection of direct-driven pmsg-based wind generators. *Electric Power Systems Research*, 151, 440–450. doi:10.1016/j.epsr.2017.06.014.

Fakham, H., Lu, D., and Francois, B. (2011). Power control design of a battery charger in a hybrid active pv generator for load-following applications. *IEEE Transactions on Industrial Electronics*, 58(1), 85–94. doi:10.1109/TIE.2010.2062475.

Guerrero, J.M., Chandorkar, M., Lee, T.L., and Loh, P.C. (2013). Advanced control architectures for intelligent microgrids—part i: Decentralized and hierarchical control. *IEEE Transactions on Industrial Electronics*, 60(4), 1254–1262. doi:10.1109/TIE.2012.2194969.

Guerrero, J.M., Vasquez, J.C., Matas, J., de Vicuna, L.G., and Castilla, M. (2011). Hierarchical control of droop-controlled ac and dc microgrids - a general approach toward standardization. *IEEE Transactions on Industrial Electronics*, 58(1), 158–172. doi:10.1109/TIE.2010.2066534.

Karimi, Y., Oraee, H., Golsorkhi, M.S., and Guerrero, J.M. (2017a). Decentralized method for load sharing and power management in a pv/battery hybrid source islanded microgrid. *IEEE Transactions on Power Electronics*, 32(5), 3525–3535. doi:10.1109/TPEL.2016.2582837.

Karimi, Y., Oraee, H., and Guerrero, J.M. (2017b). Decentralized method for load sharing and power management in a hybrid single/three-phase-islanded microgrid consisting of hybrid source pv/battery units. *IEEE Transactions on Power Electronics*, 32(8), 6135–6144. doi:10.1109/TPEL.2016.2620258.

Kazimierczuk, M.K. (2015). *Pulse-Width Modulated DC-DC Power Converters*. Wiley, 2nd edition.

Lasseter, R. (2002). Microgrids. In *2002 IEEE Power Engineering Society Winter Meeting. Conference Proceedings (Cat. No.02CH37309)*, volume 1, 305–308. doi:10.1109/PESW.2002.985003.

Mahmood, H., Michaelson, D., and Jiang, J. (2015). Decentralized power management of a pv/battery hybrid unit in a droop-controlled islanded microgrid. *IEEE Transactions on Power Electronics*, 30(12), 7215–7229. doi:10.1109/TPEL.2015.2394351.

Matos, J.G.d., e Silva, F.S.F., and Ribeiro, L.A.d.S. (2015). Power control in ac isolated microgrids with renewable energy sources and energy storage systems. *IEEE Transactions on Industrial Electronics*, 62(6), 3490–3498. doi:10.1109/TIE.2014.2367463.

Netto Moura, A.d. (2019). *Analysis of Droop Control in an Isolated Single-Phase Microgrid with Photovoltaic Generation*. Masters dissertation, Polytechnic Institute of Bragança, Bragança.

Olivares, D.E., Mehrizi-Sani, A., Etemadi, A.H., Cañizares, C.A., Iravani, R., Kazerani, M., Hajimiragha, A.H., Gomis-Bellmunt, O., Saeedifard, M., Palma-Behnke, R., Jiménez-Estévez, G.A., and Hatziargyriou, N.D. (2014). Trends in microgrid control. *IEEE Transactions on Smart Grid*, 5(4), 1905–1919. doi:10.1109/TSG.2013.2295514.

Pattabiraman, D., Lasseter., R.H., and Jahns, T.M. (2018). Comparison of grid following and grid forming control for a high inverter penetration power system. In *2018 IEEE Power Energy Society General Meeting (PESGM)*, 1–5. doi:10.1109/PESGM.2018.8586162.

Silva, Júnior, G.P.d., Barros, L.S., and Barros, C.M.V. (2021). Synchronverter coupled to a lithium-ion bank for grid frequency and voltage supports and controlled charge-discharge. *Electric Power Systems Research*, 197, 107352. doi:10.1016/j.epsr.2021.107352.

Unamuno, E. and Barrena, J.A. (2015). Hybrid ac/dc microgrids—part i: Review and classification of topologies. *Renewable and Sustainable Energy Reviews*, 52, 1251–1259. doi:https://doi.org/10.1016/j.rser.2015.07.194.

Vasquez, J.C., Guerrero, J.M., Savaghebi, M., Eloy-Garcia, J., and Teodorescu, R. (2013). Modeling, analysis, and design of stationary-reference-frame droop-controlled parallel three-phase voltage source inverters. *IEEE Transactions on Industrial Electronics*, 60(4), 1271–1280. doi:10.1109/TIE.2012.2194951.

Zhang, H., Gao, Y., and Lu, D. (2018). Micro-grid droop control strategy optimization and simulation. In *2018 China International Conference on Electricity Distribution (CICED)*, 2013–2017. doi:10.1109/CICED.2018.8592279.